JGR Earth Surface

RESEARCH ARTICLE
10.1029/2022JF006855

# Late Holocene Cliff Retreat in Del Mar, CA, Revealed From Shore Platform $^{10}$Be Concentrations and Numerical Modeling

**T. Clow[1], J. K. Willenbring[1], A. P. Young[2], H. Matsumoto[2], A. J. Hidy[3], and J. R. Shadrick[4]**

[1]Department of Geological Sciences, Stanford University, Stanford, CA, USA, [2]Scripps Institution of Oceanography, University of California San Diego, La Jolla, CA, USA, [3]Center for Accelerator Mass Spectrometry, Lawrence Livermore National Laboratory, Livermore, CA, USA, [4]Earth Science and Engineering, Imperial College London, London, UK

**Key Points:**

- Cliff retreat in Del Mar, CA, over the last two millennia is estimated at 5–12.5 cm yr$^{-1}$ using cosmogenic dating and numerical modeling
- Millennial retreat rates are consistent with modern rates in Del Mar, CA, suggesting well-constrained baseline erosive behavior
- Modeling suggests that relative sea level rise rate might exert a control on cliff retreat in Del Mar over long timescales, but more investigation is needed

**Correspondence to:**
T. Clow,
tclow@stanford.edu

**Citation:**
Clow, T., Willenbring, J. K., Young, A. P., Matsumoto, H., Hidy, A. J., & Shadrick, J. R. (2023). Late Holocene cliff retreat in Del Mar, CA revealed from shore platform $^{10}$Be concentrations and numerical modeling. *Journal of Geophysical Research: Earth Surface*, *128*, e2022JF006855. https://doi.org/10.1029/2022JF006855

Received 29 JUL 2022
Accepted 24 MAR 2023

**Author Contributions:**

**Conceptualization:** T. Clow, J. K. Willenbring, A. P. Young
**Data curation:** T. Clow, A. P. Young, H. Matsumoto
**Formal analysis:** T. Clow, A. J. Hidy
**Investigation:** T. Clow, A. P. Young
**Methodology:** T. Clow, J. K. Willenbring, H. Matsumoto, J. R. Shadrick
**Project Administration:** J. K. Willenbring
**Resources:** A. P. Young, H. Matsumoto
**Software:** H. Matsumoto, J. R. Shadrick
**Supervision:** J. K. Willenbring
**Validation:** T. Clow
**Writing – original draft:** T. Clow



**Abstract** Rocky coast cliff retreat presents a hazard to coastal communities and infrastructure that is potentially amplified under rising sea level conditions, among other factors. Unfortunately, constraints on retreat rates are typically limited to those derived from imagery and maps spanning the last ~100 years. Here, we use a newly developed coupled model of shore platform profile evolution and cosmogenic radionuclide production that considers the influence of relative sea level (RSL) rise, weathering, material resistance, and wave height decay to model cliff retreat over millennial timescales and its potential drivers in Del Mar, California. We demonstrate the ability to use topographic and bathymetric measurements from a narrow shore platform along with a limited data set of nine cosmogenic $^{10}$Be concentrations extending ~125 m from the cliff base to obtain modeled cliff retreat rates that steadily range from 5.0 to 12.5 cm yr$^{-1}$ over the last two millennia until 100 years before present. These rates are consistent with modern retreat rates of about 2–19 cm yr$^{-1}$ here. RSL rise in Southern California remained relatively constant during the late Holocene, potentially explaining the relatively stable modeled cliff retreat rate over this time. We also explore the relative influence of weathering, material resistance, and wave erosion efficacy and find that both weathering and wave-driven erosion are necessary to replicate the measured data at this location, with the latter exerting a stronger control on model acceptance, suggesting that waves may provide a possible mechanism by which RSL rise may influence coastal cliff erosion in southern California.

**Plain Language Summary** Erosion in rocky coastal environments is hazardous to coastal communities and infrastructure, but our ability to constrain how fast erosion and cliff retreat is occurring is typically limited to the last century. This limitation is problematic for understanding the full picture of coastal cliff retreat to properly mitigate risk. We use a newly developed method to estimate cliff retreat over thousands of years in Del Mar, California, where extensive infrastructure exists just tens of meters from an eroding cliff. A new data set that estimates the length of time a shore platform is exposed is combined with a model that simulates cliff retreat and shore platform development to quantify cliff retreat rates that steadily range from 5.0 to 12.5 cm yr$^{-1}$ over the last 2,000 years. This long-term rate is consistent with modern retreat rates of 2–19 cm yr$^{-1}$ over the last century here. The rate of relative sea level rise appears to have influence cliff retreat over millennial timescales here, but more detailed investigation is needed to further assess this possibility. This is the first study to use this method to determine cliff retreat rates over millennial timescales both in North America and with a limited cosmogenic data set.

## 1. Introduction

Eroding coastal cliffs are common along the world's coast (Emery & Kuhn, 1982; Young & Carilli, 2019) and are often proximal to critical infrastructure including railways, roads, and homes—hosting nearly a quarter of the global population (Small & Nicholls, 2003). In California, over 80% of the coastline is actively eroding (Griggs, 1998) and about 85% of residents either live or work near the coast (California Natural Resources Agency, 2009). Cliff retreat threatens these coastal communities, with current and projected sea level rise and increased storminess potentially exacerbating an existing coastal erosion management problem (Dickson et al., 2007; IPCC, 2021). This problem highlights the need for quantitative studies of historical cliff retreat to properly adapt to future conditions; however, quantitative studies of long-term (>100 years) cliff retreat in California are rare. This paucity of data limits incorporating the natural context of the coastline and baseline rates into future coastal evolution scenarios that often rely on relatively recent observations (e.g., Limber et al., 2018). Recent advances using cosmogenic nuclide concentrations and topographic measurements of preserved shore

**Writing – review & editing:** J. K. Willenbring, A. P. Young, H. Matsumoto, A. J. Hidy, J. R. Shadrick

platforms (e.g., M. D. Hurst et al., 2016; Regard et al., 2012; Shadrick et al., 2021; Swirad et al., 2020) provide novel methods for quantifying site-specific coastal evolution histories over long time periods not mired by human modification, modern sea level rise, and infrequent mass wasting events.

Previous work on the evolution of rocky coasts has focused on better understanding the drivers of cliff retreat and shore platform development, deciphering erosional processes from preserved platforms (e.g., D. M. Kennedy et al., 2011), the influence of setting on resulting form (e.g., Naylor et al., 2010), and geomorphic feedbacks among varying geological and climatic settings (e.g., Kline et al., 2014), most of which rely on short-term (i.e., last ∼100 years) observations of cliff failure. Cliff retreat depends on several factors, including the resistance of the material exposed to wave energy delivered to the cliff base and face. The effective energy imposed on cliffs by wave action is dependent on the incident wave conditions, nearshore wave transformation, the geometry, bedding, and jointing of the shore platform, and beach width, among other factors (Buchanan et al., 2020; Sunamura, 1992; Swirad et al., 2019; Trenhaile, 2000). Vertical erosion (downwearing) of the shore platform is also influenced by similar processes, as well as weathering from wetting and drying cycles as tides ebb and flow, bioerosion, and other factors. Together, these erosional processes that generate and dynamically link coastal cliff retreat and shore platform erosion are affected by climate, tides, lithology, structure (i.e., bedding/jointing), and sea level (D. M. Kennedy et al., 2014). Climate change adds further complexity to cliff retreat morphodynamics, again highlighting the necessity to better understand past cliff retreat in order to better inform predictive models for future cliff retreat.

### 1.1. Modern (0–100 Years Before Present) Retreat Rates

Our work is focused along the coastline of Del Mar, San Diego County, California (Figure 1), where photogrammetry, historical maps, and LiDAR-derived studies constrain the pace and tempo of seacliff erosion over the last ∼100 years before present (BP) (e.g., Hapke & Reid, 2007; Young, 2018; Young, Flick, et al., 2009; Young, Guza, et al., 2009; Young et al., 2021). Studies using historical maps and imagery often measure cliff retreat as the distance between cliff top (or cliff base) positions over time with data sources that do not extend back further than ∼150 years (Dornbusch et al., 2008; Prémaillon et al., 2018; Sunamura, 1992). In San Diego County, rates from the 1930s to present are variable, averaging from 4 to 25 cm $yr^{-1}$, but can exceed 400 cm $yr^{-1}$ (Young, 2018). The most dramatic recent rates are associated with deep-seated, complex coastal landslides near San Onofre (Young, 2015). Typical average decadal cliff retreat rates at Del Mar are estimated at 2–19 cm $yr^{-1}$ (Figure 2, Benumof & Griggs, 1999; Hapke & Reid, 2007; Moore et al., 1999; Swirad & Young, 2022; Young, 2018; Young & Ashford, 2006; Young, Flick, et al., 2009; Young et al., 2021). Constraining cliff retreat in Del Mar is of particular interest in the southern California area as a major railroad is located within a few meters of the cliff edge (Figure 1), with episodic cliff failures resulting in several derailments in modern history (Kuhn & Shepard, 1984). In the 20th century, Kuhn and Osborne (1987) anecdotally observed that many of the coastal cliff mass wasting events in San Diego occurred during above-average rainfall events that likely saturate the cliffs. Recent work also indicates that rainfall and cliff erosion are statistically correlated in San Diego, along with wave impact to a roughly equal degree (Young et al., 2021). Specifically, Young et al. (2021) found that in modern times, lower cliff face erosion significantly correlates with wave impact and duration, while upper cliff face erosion correlates with periods of rainfall. Young, Guza et al. (2009) also highlighted the compounding nature of wave impact, showing that segments of the cliff base exposed to wave attack show a five-fold increase in modern cliff retreat than those not.

Decadal cliff retreat rates and observations only provide a snapshot of the most recent changes due to the inherent limitations of historical records and photography (Brooks & Spencer, 2010); thus, we are left with records that are often affected by the influence of anthropogenic modification including coastal development and infrastructure, cliff base armoring, and beach nourishment (e.g., Flick, 1993; Willis & Griggs, 2003; Young et al., 2010). Researchers have also noted that averaging timescale has an influence on the magnitude and variance of rates (McElroy et al., 2018). In this setting, infrequent large-scale cliff failure events might either be missed or perhaps dominate the observational period (Young, 2018) and thus might not capture long-term trends and fluctuations. These factors complicate using modern records to forecast future cliff retreat (Sunamura, 2015; Young, 2018), highlighting the necessity for longer term cliff retreat rate estimates that include multiple cycles of mass wasting events, climatic shifts, and known relative sea level rise.

### 1.2. Estimating Long-Term Retreat Rates

In this study, we complement and provide further context to modern cliff retreat studies in Del Mar by quantifying the late Holocene cliff retreat history using a newly developed modeling approach (Shadrick et al., 2021)

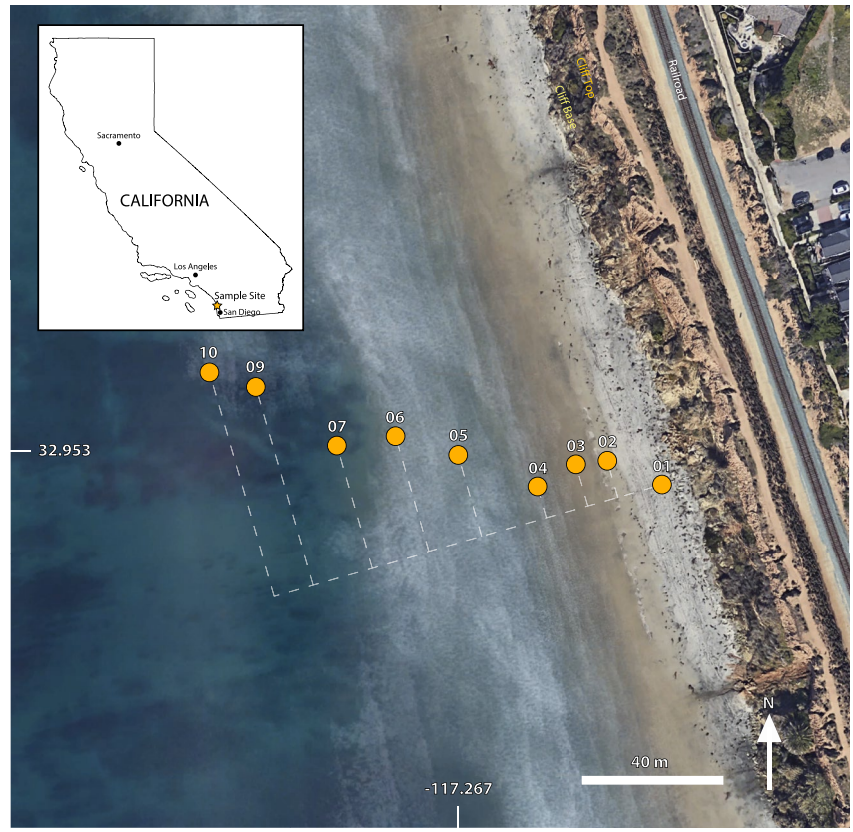


**Figure 1.** Aerial map of the study area and sampling transect in Del Mar, California (courtesy of Google Earth). Orange circles show the location of cosmogenic samples gathered on the shore platform (obscured by sand and ocean water in this image); sample number increases with distance from the shore. Dashed lines show correction to a cliff perpendicular transect used to constrain absolute distance from cliff base. Cliff base and cliff top are delineated with yellow and orange lines, respectively. See Table 4 for precise sample elevations and distances used in the model.

that combines two data sources: new cosmogenic $^{10}$Be concentrations and topographic and bathymetric measurements from $a > 125$ m wide shore platform. We exploit the production of a cosmogenic radionuclide, in situ-produced $^{10}$Be (half-life 1.39 ± 0.01 Myr, Chmeleff et al., 2010; Korschinek et al., 2010), that occurs as cosmic rays interact with target elements (i.e., $^{16}$O and $^{14}$N) in quartz crystals at and near Earth's surface to determine the previous exposure history of the shore platform. Cosmogenic $^{10}$Be builds up over time, but erosion reduces observed surface concentrations (Lal, 1991). There are two primary pathways of $^{10}$Be production: production from spallogenic reactions (~4 atoms g$^{-1}$ yr$^{-1}$ at sea level high latitude [SLHL]), which dominates production in the uppermost 1–2 m of Earth's surface where secondary neutrons are effectively stopped, and production from deeply penetrating muons (0.028 atoms g$^{-1}$ yr$^{-1}$ at SLHL), which dominate production at much greater depths, despite its comparatively lower production rate, due to its ~26x longer attenuation length compared to spallation (Braucher et al., 2003). In both pathways, in situ-produced $^{10}$Be production decreases approximately exponentially with depth below Earth's surface due to attenuation of the cosmic ray flux through mass (Gosse & Phillips, 2001). Constraining the exposure history of the platform using measured shore platform $^{10}$Be concentrations and estimating a long-term retreat rate requires a numerical model of shore platform development that considers the range of factors that influence cosmogenic $^{10}$Be production over time.

To quantify long-term cliff retreat rates, we utilize a multiobjective optimization (Shadrick et al., 2021) of a coupled coastal evolution model that combines an exploratory process-based Rocky Profile Model (RPM) of rocky coast erosion and shore platform development (Matsumoto et al., 2016) along with a process-based rocky coast cosmogenic radionuclide production model (RoBoCoP) (M. D. Hurst et al., 2017). These models build considerably on previous exploratory models (Sunamura, 1992; Trenhaile, 2000, 2008) and further allow us to better constrain the environmental and erosional processes that control the development of the shore platform,

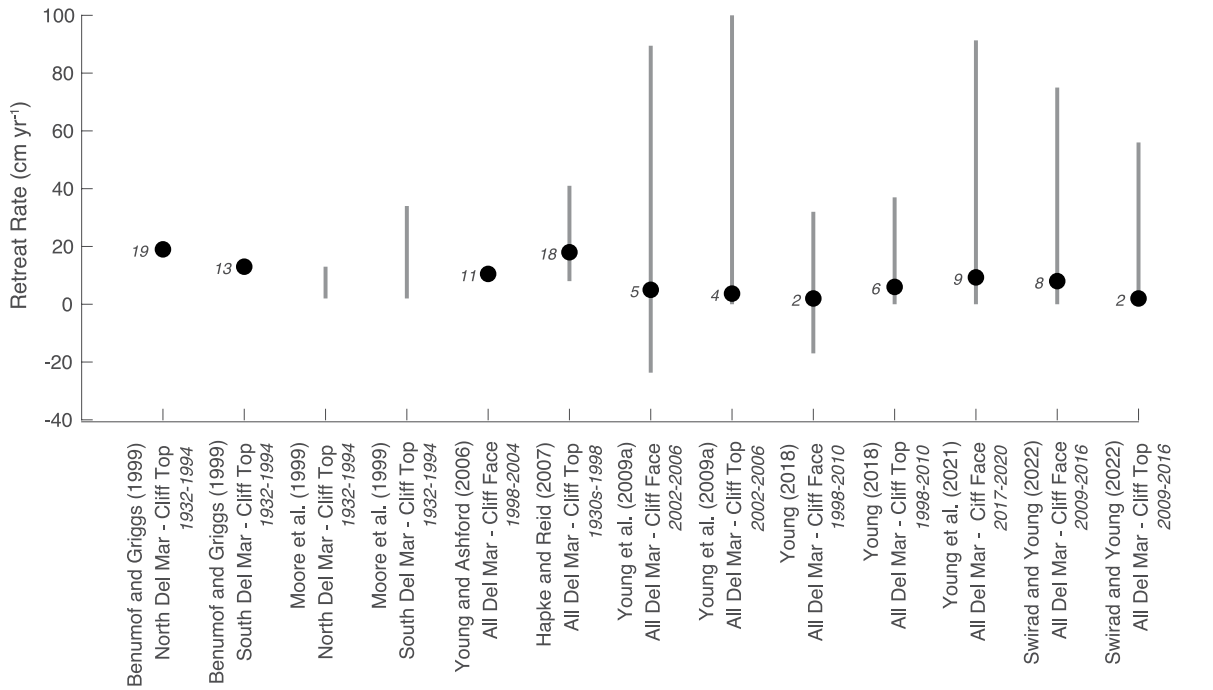


**Figure 2.** Rates of modern coastal cliff retreat in Del Mar, California. Time interval over which modern cliff retreat rates were determined are reported for each study, along with the point of reference (i.e., cliff top or cliff face) used to calculate retreat rates. Dots represent the mean rates in cm $yr^{-1}$ (where reported) for each study. Bars represent ranges in retreat rates for each study (where reported). Modern cliff retreat rate ranges determined by cliff face measurements may include negative rates due to net accumulation of colluvium at the cliff face/base. See references for more details.

but have yet to be explored with a limited cosmogenic data set from a relatively narrow spatial extent. Successful implementation of this coupled model approach will allow for the constraint of the long-term geomorphic evolution of rocky coasts over a wide range of coastal cliff environments (and degree of shore platform preservation therein) in a manner that reduces equifinality that often arises from coastal evolution models due to (necessarily) simplified erosional processes (Shadrick et al., 2021). Best fit solutions are achieved via Metropolis Hastings Markov Chain Monte Carlo (MCMC, Adams et al., 2019; Estacio-Hiroms et al., 2016) simulations that iterate over a wide range of possible input values for the parameters most likely to influence shore platform evolution: material resistance, wave height decay rate, and intertidal weathering rate (Carr & Graff, 1982; Matsumoto et al., 2018), Through a simultaneous optimization of measured $^{10}$Be concentrations and shore platform topography to modeled predictions of both, we estimate late Holocene (~2 kyr) coastal cliff retreat rates for Del Mar, California and explore the influence of relative sea level rise, waves, and weathering on long-term coastal erosion at this site.

### 1.3. Site Details

Coastal Del Mar, California, located in San Diego County, California, is situated on a ~15–30-m-tall cliff (~23 m at this study site) that is cut into sedimentary deposits (Figure 3a). The lower cliff is composed of the Eocene-age (37–54 Myr), sedimentary Del Mar Formation, characterized as a sandy claystone interbedded with coarse-grained sandstone (Figure 3a, M. P. Kennedy, 1975; Young et al., 2010). This locally relatively impermeable claystone is overlain by sandy Pleistocene terrace deposits that are ~10 m thick at this study site. This interface presents an opportunity for perched groundwater and sapping to influence cliff top stability, whereas the cliff base is subject to wave attack, particularly in winter months where the beach width is narrower than in the summer (Ludka et al., 2019; Young, Flick, et al., 2009). The cliff face is also subject to subaerial weathering, dessication, rilling, and other erosional processes (Young, Guza, et al., 2009; Figure 3a).

San Diego County is host to a semiarid Mediterranean climate with dry summers and comparatively wet winters. Total annual rainfall in Del Mar, CA ranges between 10–60 cm (mean 25 cm), most of which occurs between November and March (Young, Guza, et al., 2009; Young et al., 2021), with episodic winter storms often delivering a large portion of the rainfall budget. The episodic nature of above-average precipitation events has been noted to


**Figure 3.** (a) Photograph of the cliff (~23 m tall) in Del Mar, CA; lower cliff is composed of Eocene-age Del Mar formation sandy claystone and is mostly obscured by talus deposits from recent rock fall events, upper cliff is Pleistocene terrace deposits showing evidence of rilling. (b) Photograph of shore platform taken ~110 m from cliff base, showing vegetation and the patchy preservation of the shore platform with increasing distance from the cliff. (c) A sampled sandstone nodule (CA-19-DLM02) located on the shore platform.

influence coastal landsliding in the area over recent decadal observational periods, particularly during El Niño years (e.g., 1982–1983, 1997–1998) and the wet winter of 2004–2005 (Kuhn & Osborne, 1987; Young, Flick, et al., 2009). Mean wave height is 1.07 in 17 m water depth offshore of Del Mar (CDIP Buoy 153, http://cdip.ucsd.edu/) and the tide (MLLW-MHHW) ranges up to about 1.1 m (La Jolla Station ID 9410230, https://tidesandcurrents.noaa.gov).

Quantifying cliff retreat over millennial timescales rate using cosmogenic nuclides and numerical modeling relies on the existence of a shore platform upon which the cliff has retreated. This study site presents a unique opportunity to utilize cosmogenic radionuclide concentrations to quantify the history of exposure and retreat in an area with limited shore platform preservation/exposure, utilizing $a > 125$ m wide portion of an in-place, nearly horizontal ($\tan \beta = 0.0116$) shore platform, also composed of the Del Mar Formation sandy claystone (Figures 1 and 3b). Near the cliff base, this platform is typically obscured by sand during the summer months, while in the winter the platform is sometimes well exposed, particularly during low tide. Thickness of beach sand is variable throughout the year, ranging from a couple meters thick in the summer to absent during the winter and generally thickens closer to the cliff base (Young et al., 2016). Beach sand overburden creates the potential for attenuation of the cosmogenic signal that could affect cosmogenic production rates and concentrations (M. D. Hurst et al., 2016, 2017; see Section 4.2 for details). Distal from the cliff, the shore platform becomes more patchy with an increasing concentration of mollusk burrows and vegetation (seagrass) toward the sea (Figure 3b). While their effect on the density of the claystone (~2.1 g $cm^{-3}$) is minor, boring from mollusks presents the opportunity for bioerosion that acts to reduce the material resistance and resisting force of the shore platform (Naylor et al., 2012).

### 1.4. Uplift, Glacial Isostatic Adjustment, and Sea Level Change in San Diego County

Tectonic uplift and glacial isostatic adjustment influence the relative magnitude of sea level rise (or fall) in coastal environments, which in turn affects our ability to accurately resolve the influence of sea level rise on coastal erosion. Sea level rise influences the magnitude of water cover above the shore platform, which partially

**Table 1**
*Model Input Relative Sea Level for Del Mar, CA*

| Time (years BP) | RSL (m) |
|---|---|
| 8,000 | −10.16 |
| 7,000 | −8.24 |
| 6,000 | −6.32 |
| 5,000 | −4.84 |
| 4,000 | −3.36 |
| 3,000 | −2.56 |
| 2,000 | −1.76 |
| 1,000 | −0.96 |
| 100 | −0.16 |
| 0 | 0 |

*Note*. Data from Reynolds and Simms (2015) and Muhs et al. (2012); refer to Figure 5 for a graphical depiction.

shields it from secondary cosmic flux and reduces the rate of $^{10}$Be production. Thus, relative sea level needs to be characterized in parallel with cliff erosion to fully interpret $^{10}$Be that accumulated during the complex exposure history of the shore platform, as is carried out in similar studies in coastal areas characterized by slowly rising seas (e.g., M. D. Hurst et al., 2016; Shadrick et al., 2021). Coastal uplift rates for San Diego County over the Quaternary are ∼0.13 m kyr$^{-1}$, primarily determined from U-series ages of corals and amino acid dates from material from a suite of <1 Myr old marine terraces in the San Diego area (Kern & Rockwell, 1992). We utilize uplift-corrected and Glacial Isostatic Adjustment (GIA-) applied Holocene sea level rise estimates for southern California (Muhs et al., 2012; Reynolds & Simms, 2015) which indicate rapid relative sea-level rise of ∼8 mm yr$^{-1}$ until ∼8,000 years BP that then decelerates until reaching an approximately constant rate of 0.8 ± 0.3 mm yr$^{-1}$ from ∼4,000 years BP until the 20th century, after which the relative sea level rise rate approximately doubled, reaching 1.6–2.4 mm yr$^{-1}$ at present (Table 1).

## 2. Methods

### 2.1. Sampling Strategy and Preparation

Nine samples from the exposed shore platform were gathered on days of exceptionally low tide out to ∼125 m along a roughly cliff perpendicular transect (Figures 1 and 3c)—deviations from perpendicular were a result of variable preservation of suitable samples and, distal from the cliff base, fully intact and accessible shore platform and are corrected for in our distance calculations. We targeted resistant coarse sandstone nodules (containing coarse quartz grains) for cosmogenic $^{10}$Be sampling, where possible, and sampled the upper ∼5 cm of the platform/nodules, taking care to avoid potholes and densely vegetated areas (Figures 3b and 3c). Three Real Time Kinematic and Differential GPS (RTK-DGPS) measurements were acquired at each of the sample locations and combined with bathymetric measurements of the shore platform further offshore to constrain the topographic profile and gradient of the shore platform (Table 2). RTK-DGPS and bathymetric measurements both use the NAVD88 vertical datum. To constrain the potential for inheritance in our shore profile samples, we also gathered a bedrock sample at a nearby beach cave in Del Mar, California, just north of our sampling transect.

Cosmogenic samples were physically prepared via crushing, milling, and sieving the sampled material to a 250–500 μm size fraction, then purified to isolate and etch quartz following an adaptation of the standard technique developed by Kohl and Nishiizumi (1992). Purity was confirmed via microscope; all remaining nonquartz material was removed by hand via tweezers. To measure the $^{10}$Be concentration, ∼0.2 g of $^{9}$Be carrier (1,074 ± 8 ppm) was added to the 50–100 g aliquots of quartz. Beryllium was separated from other elements following the procedure of von Blanckenburg et al. (2004). Samples were then precipitated as BeOH, oxidized over a flame to convert to BeO, then packed with niobium into stainless steel targets for $^{10}$Be/$^{9}$Be analysis at the Center for Accelerator Mass Spectrometry at Lawrence Livermore National Laboratory. All ratios were measured against isotopic standard 07KNSTD3110 (ICN 01-5-4), which has a well-characterized ratio of $^{10}$Be/$^{9}$Be = 2,850 × 10$^{-15}$ (Nishiizumi et al., 2007). Nuclide concentrations were corrected for machine as well as chemistry blanks. The reported error includes analytical uncertainties at 1$\sigma$.

### 2.2. Beach Sand Thickness

Beach sand in Del Mar, California is seasonally variable and has the potential to influence the cosmogenic production rate and our treatment of accounting for cosmogenic inheritance in our shore platform samples. Two Hundred One cross-shore profiles of beach sand thickness and beach width ∼1 km north of our sampled transect were gathered between 2017 and 2022 (Young et al., 2021) to constrain average monthly thicknesses to better evaluate the potential for cosmogenic attenuation effects.

**Table 2**
*Topographic and Bathymetric Elevation Measurements for Del Mar Transect*

| Dist. (m) | Elev. (m asl) | Dist. (m) | Elev. (m asl) | Dist. (m) | Elev. (m asl) | Dist. (m) | Elev. (m asl) | Dist. (m) | Elev. (m asl) | Dist. (m) | Elev. (m asl) | Dist. (m) | Elev. (m asl) |
|---|---|---|---|---|---|---|---|---|---|---|---|---|---|
| 1 | 0.67 | 31 | −0.27 | 61 | −0.89 | 91 | −1.30 | 121 | −1.34 | 151 | −1.51 | 181 | −1.98 |
| 2 | 0.64 | 32 | −0.30 | 62 | −0.91 | 92 | −1.30 | 122 | −1.34 | 152 | −1.51 | 182 | −2.02 |
| 3 | 0.61 | 33 | −0.32 | 63 | −0.94 | 93 | −1.29 | 123 | −1.35 | 153 | −1.52 | 183 | −2.06 |
| 4 | 0.57 | 34 | −0.35 | 64 | −0.96 | 94 | −1.29 | 124 | −1.35 | 154 | −1.52 | 184 | −2.10 |
| 5 | 0.54 | 35 | −0.37 | 65 | −0.99 | 95 | −1.29 | 125 | −1.35 | 155 | −1.52 | 185 | −2.14 |
| 6 | 0.51 | 36 | −0.39 | 66 | −1.01 | 96 | −1.29 | 126 | −1.36 | 156 | −1.53 | 186 | −2.18 |
| 7 | 0.48 | 37 | −0.42 | 67 | −1.03 | 97 | −1.29 | 127 | −1.36 | 157 | −1.53 | 187 | −2.21 |
| 8 | 0.45 | 38 | −0.44 | 68 | −1.05 | 98 | −1.29 | 128 | −1.37 | 158 | −1.54 | 188 | −2.25 |
| 9 | 0.41 | 39 | −0.46 | 69 | −1.08 | 99 | −1.28 | 129 | −1.38 | 159 | −1.54 | 189 | −2.29 |
| 10 | 0.38 | 40 | −0.48 | 70 | −1.10 | 100 | −1.28 | 130 | −1.38 | 160 | −1.55 | 190 | −2.33 |
| 11 | 0.35 | 41 | −0.50 | 71 | −1.12 | 101 | −1.28 | 131 | −1.39 | 161 | −1.55 | 191 | −2.36 |
| 12 | 0.32 | 42 | −0.52 | 72 | −1.14 | 102 | −1.28 | 132 | −1.40 | 162 | −1.56 | 192 | −2.40 |
| 13 | 0.29 | 43 | −0.54 | 73 | −1.15 | 103 | −1.28 | 133 | −1.41 | 163 | −1.56 | 193 | −2.43 |
| 14 | 0.25 | 44 | −0.56 | 74 | −1.17 | 104 | −1.28 | 134 | −1.41 | 164 | −1.57 | 194 | −2.47 |
| 15 | 0.22 | 45 | −0.58 | 75 | −1.19 | 105 | −1.28 | 135 | −1.42 | 165 | −1.58 | 195 | −2.50 |
| 16 | 0.19 | 46 | −0.60 | 76 | −1.20 | 106 | −1.28 | 136 | −1.43 | 166 | −1.59 | 196 | −2.53 |
| 17 | 0.16 | 47 | −0.62 | 77 | −1.22 | 107 | −1.29 | 137 | −1.44 | 167 | −1.60 | 197 | −2.56 |
| 18 | 0.13 | 48 | −0.63 | 78 | −1.23 | 108 | −1.29 | 138 | −1.44 | 168 | −1.62 | 198 | −2.60 |
| 19 | 0.10 | 49 | −0.65 | 79 | −1.24 | 109 | −1.29 | 139 | −1.45 | 169 | −1.63 | 199 | −2.63 |
| 20 | 0.07 | 50 | −0.67 | 80 | −1.25 | 110 | −1.29 | 140 | −1.45 | 170 | −1.65 | 200 | −2.66 |
| 21 | 0.03 | 51 | −0.69 | 81 | −1.26 | 111 | −1.30 | 141 | −1.46 | 171 | −1.67 | | |
| 22 | 0.00 | 52 | −0.70 | 82 | −1.27 | 112 | −1.30 | 142 | −1.46 | 172 | −1.69 | | |
| 23 | −0.03 | 53 | −0.72 | 83 | −1.28 | 113 | −1.30 | 143 | −1.47 | 173 | −1.72 | | |
| 24 | −0.06 | 54 | −0.74 | 84 | −1.28 | 114 | −1.31 | 144 | −1.47 | 174 | −1.74 | | |
| 25 | −0.09 | 55 | −0.76 | 85 | −1.29 | 115 | −1.31 | 145 | −1.48 | 175 | −1.77 | | |
| 26 | −0.12 | 56 | −0.78 | 86 | −1.29 | 116 | −1.32 | 146 | −1.48 | 176 | −1.80 | | |
| 27 | −0.15 | 57 | −0.80 | 87 | −1.30 | 117 | −1.32 | 147 | −1.49 | 177 | −1.83 | | |
| 28 | −0.18 | 58 | −0.82 | 88 | −1.30 | 118 | −1.32 | 148 | −1.49 | 178 | −1.87 | | |
| 29 | −0.21 | 59 | −0.85 | 89 | −1.30 | 119 | −1.33 | 149 | −1.50 | 179 | −1.90 | | |
| 30 | −0.24 | 60 | −0.87 | 90 | −1.30 | 120 | −1.33 | 150 | −1.50 | 180 | −1.94 | | |

### 2.3. Coastal Evolution Modeling

Constraining long-term cliff retreat rates using cosmogenic surface exposure dating requires numerical modeling to interpret the concentrations appropriately. Without accounting for water and topographic shielding, which effectively reduce the site-specific cosmogenic production rate over time, erroneously high retreat rates will manifest. Additionally, as evidence of the developmental stages of the erosional evolution of rocky coasts are rarely preserved, numerical models are necessary for investigating shore profile development and their drivers. We use a multiobjective optimization of a coupled process-based numerical model of cosmogenic radionuclide production and shore platform topographic evolution (M. D. Hurst et al., 2017; Matsumoto et al., 2016; Shadrick et al., 2021) to minimize residuals between model results and measured data, resulting in a best-fit solution. A full explanation of each model is beyond the scope of this paper and can be found in the respective references; however, the pertinent details of each model are discussed below.

**Table 3**
*Markov Chain Monte Carlo Simulation and Model Inputs for Del Mar Site*

| Category | Model input | Value |
|---|---|---|
| MCMC Dakota | Proposal covariance | 0.5 |
| | Topographic scale | 0.68 |
| | $^{10}$Be scale | 541 |
| Tides | Tidal range (m) | 1.1 |
| | Tidal period (hr) | 12.42 |
| | Mean wave height (m) | 1.1 |
| Waves | Standing coefficient | 0.1 |
| | Breaking coefficient | 10 |
| | Broken coefficient | 1 |
| | Cliff failure depth (m) | 0.1 |
| General RPM | Initial gradient (tan $\beta$) | 1 |
| | Cell resolution (m) | 0.1 |

#### 2.3.1. Details of the Rocky Profile Model

In the RPM (Matsumoto et al., 2016), cliff retreat and shore platform development are governed by erosional driving and modulating processes and are simulated via a grid discretization framework with each cell classified as either rock or water/air. Cliff erosion creates a shore platform that widens over time, which in turn causes wave energy dissipation and reduces cliff erosion (e.g., Trenhaile, 2000). Wave erosion and intertidal weathering are primary erosion-driving processes, while material resistance affects the rate and magnitude of erosion. Wave erosion occurs when wave assailing force exceeds the material resistance of rocks (Sunamura, 1992), which turns rock cells into water/air cells within the model space. Two types of wave assailing force are considered: horizontal backwear and vertical downwear, and are estimated using factors such as wave height, wave height decay rates, and the tidal duration distribution (Carr & Graff, 1982). Intertidal weathering reduces the material resistance of intertidal surface rocks. Following studies of wetting and drying patterns on shore platforms (e.g., Kanyaya & Trenhaile, 2005), intertidal weathering has its peak efficacy at mean high water neap elevation with efficacy decreasing above and below this level. As this suite of processes progresses over time, shore platform topography is modeled for comparison against measured topography.

#### 2.3.2. Details of RoBoCoP

In RoBoCoP (M. D. Hurst et al., 2017), cosmogenic radionuclide production and accumulation on eroding shore platforms is modeled by calculating the concentration of $^{10}$Be via spallation (at- and near-surface) and deep-penetrating muon production (at depth) for each rock cell over time to account for the evolution of both horizontal (retreat) and vertical (down-wearing) erosion of the cliff-shore platform interface. As the cliff retreats and new shore platform is exposed to cosmic rays, $^{10}$Be is produced primarily through spallation reactions, which dominate the production signal. Thus, $^{10}$Be concentrations will accumulate and increase offshore from the cliff base as additional rock is removed. However, platform lowering and intertidal weathering act to remove the uppermost layer of rocks that contain higher $^{10}$Be concentrations compared to that underneath, with the new baselevel surface now subject to higher production rates. As rock cells are eroded and become water/air cells within the model space, a sawtooth pattern in the modeled cosmogenic nuclide profile emerges due to the revealing of these new cells (resolution = 10 × 10 cm) with comparatively lower $^{10}$Be concentration. RoBoCoP considers shielding of the incident cosmic rays from water cover across the platform, which is modulated by sea level rise and tides, whereby an exponential increase in cosmic ray flux attenuation occurs as water depth increases offshore, leading to reduced $^{10}$Be production over time (M. D. Hurst et al., 2017), but beach cover is not considered in the implementation of RoBoCoP in the coupled model which may affect the production rate by as much at ∼15% at this location (see Section 4.2). This process leads to a characteristic "hump", or peak, in $^{10}$Be concentration against distance from the cliff base (M. D. Hurst et al., 2016; Regard et al., 2012). Additionally, topographic shielding of the shore platform from the seacliff itself is considered in the model, which primarily affects cosmogenic production at and near the position of the cliff base as the platform evolves.

#### 2.3.3. Coupled Model Implementation

In practical terms, estimating retreat rates in this framework is achieved by specifying known present-day measurements (cliff height, tidal range, uplift-corrected and GIA-applied sea level rise, wave height; Table 3) as estimated input initial conditions. Then, by varying values for wave height decay rate ($y$, m$^{-1}$), material resistance ($Fr$, kg m$^{-2}$ yr$^{-1}$), and intertidal weathering rate ($K$, kg m$^{-2}$ yr$^{-1}$), the resulting modeled $^{10}$Be concentrations and platform geometries are compared against the measured $^{10}$Be concentrations and shore platform topography simultaneously in a coupled framework (Shadrick et al., 2021). The shore platform evolution model considers mean sea level (msl) to be zero (Matsumoto et al., 2016); therefore, measured topographic and bathymetric data collected using the NAVD88 vertical datum were converted to relative msl elevations. Best-fit solutions are determined using a multiobjective model optimization of this coupled model, summarized below.

Multiobjective model optimization is achieved by a Metropolis Hastings MCMC via Dakota optimization software (Adams et al., 2019) with the QUESO Bayesian calibration library (Estacio-Hiroms et al., 2016), first presented by Shadrick et al. (2021). The MCMC is utilized to establish the best-fit model parameters for wave height decay rate ($y$), material resistance (Fr), and intertidal weathering rate ($K$) that lead to the lowest combined root mean square error (RMSE) scores for measured versus modeled cosmogenic radionuclide concentrations and shore platform topography, representing the highest likelihood estimation for this site, as determined from the Dakota-calculated composite likelihood scores for each simulation in the MCMC. These three parameters were chosen to vary as previous investigation has shown that they have large propensity to influence coastal evolution and resulting form (Matsumoto et al., 2018). Using a uniform prior distribution for these parameters, necessary as we have no a posteriori knowledge of the best-fit model parameters, we aim for an acceptance rate of ∼23% to fully explore the parameter space (Gelman et al., 1997; Shadrick et al., 2021). Our goal is to determine best-fit modeled solutions that most closely match the observed cosmogenic concentrations and shore platform topography, not which parameters most closely match real-world values (Shadrick et al., 2021). When a combination of parameters does not sufficiently replicate the measured topographic profile (i.e., when the modeled topographic profile is not at least the width of the measured topographic profile), a "fail" flag is returned, allowing future simulations within the MCMC to avoid such parameter combinations. A more detailed explanation of the MCMC analysis and the functionality of Dakota is presented in Shadrick et al. (2021).

We fully explore the parameter space by allowing the model to iterate over multiple orders of magnitude by varying the exponent factor for each variable ($a$ for $y$, $b$ for $Fr$, $c$ for $K$), which are treated as the calibration parameters for model optimization. The range in exponents ($-2 < a < 0.8$; $1 < b < 3$; $-8 < c < 1$), and thus parameter space, was primarily selected based on field experiments (e.g., Ogawa et al., 2011 for wave height decay rate) and the ranges previously explored by Matsumoto et al. (2018) and Shadrick et al. (2021) which replicated a large range in platform geometries and optimal MCMC acceptance rates (Gelman et al., 1997), respectively. Material resistance ($Fr = 10^b$) is allowed to vary from 10 to 1,000 kg $m^{-2}$ $yr^{-1}$, which is comparable to rock resistance values used by Matsumoto et al. (2018) and Trenhaile (2000, 2008) and encapsulates the variability in material resistance owing to geological/lithological/structural factors (e.g., Sunamura, 1994). Wave height decay rate ($y = 10^a$) varies from 0.01 to 0.16 $m^{-1}$. Intertidal weathering rate ($K = 5^c \times Fr$), which varies as a proportion of material resistance, varies from $10^{-5}$ to 1,000 kg $m^{-2}$ $yr^{-1}$ in order to encompass weathering rates well past the upper end of those expected for sandstone platforms (Yuan et al., 2020), as well as negligible weathering rates (i.e., the weathering rate is much less than material resistance, whereby rocks cannot be eroded by weathering alone).

We allow the model to run for 8,000 years, with a step size of 100 years, which encapsulates the history of the initially rapid rate of RSL rise that declines and ultimately stabilizes until ∼100 years BP in the southern California region (Table 1). Previous work (and our trial runs) indicates that running the model for longer than 8,000 years (including a burn-in period) shows no change in model result over the time period of interest (Shadrick et al., 2021), which allows us to reduce lengthy computational times. There is a burn-in period of ∼1,000 years after which initial conditions such as incipient profile gradient, which is unknown, do not affect resulting platform topography; as such, we only consider cliff retreat rates after this burn-in period. We implement a relative scaling of 0.3 m and 500 atoms $g^{-1}$ for topographic and $^{10}$Be RMSE scores (RMSE; higher scores reflect greater error), respectively, which results in RMSE scores of comparable magnitude for both the topographic profile and cosmogenic radionuclide concentrations and thus lower combined RMSE scores, as determined from multiple trial $n = 1000$ MCMC runs at different scales. We chose to assign an equal weighting (50%–50%) of topographic and $^{10}$Be RMSE scores in our MCMC calculations, which provided the best-fit model results out of all possible weighting scenarios in Shadrick et al. (2021). Uncertainties ($1\sigma$) for the best-fit parameter values are determined by the 16%, 50%, and 84% confidence intervals of only the accepted MCMC samples. Uncertainties for the resulting modeled shore platform topography profiles, cosmogenic radionuclide profiles, and ultimately the range in modeled cliff retreat rates are determined by calculating and plotting the results of the 16%–84% confidence range for each parameter against the median result for the other two parameters, leading to six outputs (Shadrick et al., 2021). An additional model result is generated by calculating and plotting the output using the best-fit results for all three parameters (i.e., the results that produced the lowest RMSE scores). Cliff retreat rates are calculated at every 100 years interval, allowing us to determine retreat rate changes from 7,000 to 100 years BP. In total, 10,000 simulations were conducted.

**Table 4**
*Shore Platform Topography and In Situ-Produced $^{10}$Be Concentrations, Del Mar, CA*

| Sample | Distance from Cliff[a] (m) | Elevation (m asl) | $^{10}$Be sample weight (g) | $^{9}$Be carrier weight (mg) | $^{10}$Be/$^{9}$Be | $^{10}$Be/$^{9}$Be uncertainty | $^{10}$Be concentration[b] (atoms g$^{-1}$) | Inheritance-corrected $^{10}$Be concentration[c] (atoms g$^{-1}$) | $^{10}$Be concentration uncertainty (atoms g$^{-1}$) |
|---|---|---|---|---|---|---|---|---|---|
| DLM19-01 | 7.98 | 1.575 | 49.96737 | 0.23098 | 1.680E−14 | 5.942E−16 | 4,496 | 0 | 157 |
| DLM19-02 | 20.12 | 0.654 | 96.60205 | 0.23074 | 3.035E−14 | 1.345E−15 | 4,486 | 0 | 197 |
| DLM19-03 | 29.22 | 0.509 | 96.2713 | 0.23067 | 3.125E−14 | 1.112E−15 | 4,644 | 153 | 167 |
| DLM19-04 | 41.81 | 0.228 | 79.90621 | 0.23043 | 3.388E−14 | 1.695E−15 | 6,094 | 1,604 | 305 |
| DLM19-05 | 61.21 | 0.015 | 96.23285 | 0.23049 | 4.370E−14 | 1.062E−15 | 6,634 | 2,143 | 159 |
| DLM19-06 | 77.6 | −0.04 | 96.46617 | 0.23091 | 4.112E−14 | 1.609E−15 | 6,218 | 1,727 | 243 |
| DLM19-07 | 93.86 | −0.05 | 99.76673 | 0.23034 | 4.631E−14 | 1.951E−15 | 6,797 | 2,307 | 285 |
| CA-20-DLM09 | 112.52 | −0.034 | 81.74256 | 0.23139 | 4.243E−14 | 1.162E−15 | 7,617 | 3,125 | 206 |
| CA-20-DLM10 | 123.79 | −0.09 | 81.73196 | 0.23143 | 4.700E−14 | 1.235E−15 | 8,486 | 3,995 | 221 |
| CA-20-DLM11 | *Shielded* | 2.115 | 82.0189 | 0.23111 | 3.288E−14 | 1.306E−15 | 5,783 | – | 231 |

*Note.* Distance, elevation, and inheritance-corrected $^{10}$Be concentrations are model inputs.
[a]Corrected to represent distance perpendicular from cliff base. [b]Corrected for blank, reported error includes analytical uncertainties ($1\sigma$). [c]Inheritance constrained by the average concentrations of CA-19-DLM-01 and CA-19-DLM-02.

## 3. Results

### 3.1. Cosmogenic $^{10}$Be Concentrations

Measured $^{10}$Be concentrations generally increase with distance from the cliff, with concentrations ranging from ~4.49 ± 0.16 × $10^3$ at g$^{-1}$ to ~8.49 ± 0.22 × $10^3$ atoms g$^{-1}$ (Table 4). A slight decrease in concentration is observed between samples CA-19-DLM06 and CA-19-DLM07 though concentrations overlap within uncertainty, after which the trend of increasing concentration with distance resumes. Inheritance-corrected concentrations (constrained by the average concentration between CA-19-DLM01 and CA-19-DLM-02) range from 0 to ~4.0 ± 0.22 × $10^3$ at g$^{-1}$ (Table 4; Figure 5).

#### 3.1.1. Cosmogenic $^{10}$Be Inheritance

To constrain any production of $^{10}$Be that has occurred prior to the exposure of the shore platform due to deep-penetrating muons, we utilize the lowest concentration gathered from our sampling transect, constrained by the average concentration between CA-19-DLM01 and CA-19-DLM02. In theory, the concentration of the sample closest to the cliff base should effectively be zero as it has only recently been exposed to spallation reactions via cosmogenic rays; however, the concentrations of three samples nearest the cliff base are all roughly the same (~4,500 atoms g$^{-1}$), indicating that a substantial portion of the cosmogenic signal acquired in each sample is due to inheritance. To better constrain the potential for inheritance, we also gathered a bedrock sample at a nearby beach cave in Del Mar, California, just north of our sampling transect (Table 3). This sample has a concentration that exceeds that of the first three near-cliff base samples of our sampling transect by ~30%. This beach cave sample is ~1.5 m asl higher than the near-cliff base samples and has less thick overburden (~18 m asl) compared to our sampled transect (~23 m asl), which likely explains the observed discrepancy in raw $^{10}$Be concentration. For example, given a surface muon production rate of 0.028 atoms g$^{-1}$ yr$^{-1}$, an estimated attenuation length of 4,000, and a density of 2 g cm$^{-3}$, after ~500 kyr, we would expect to have ~4,400 atoms g$^{-1}$ with 23 m overburden compared to ~5,700 atoms g$^{-1}$ with 18 m of overburden, representing a ~30% increase. Regardless, the fact that this beach cave sample $^{10}$Be concentration exceeds that of the samples closest to the cliff-base indicates that the maximum possible inheritance for this

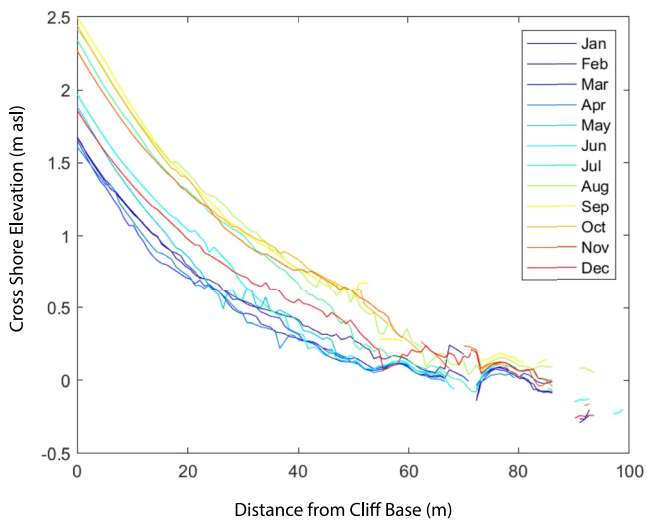


**Figure 4.** Monthly average cross shore profile elevation (m asl) from 2017 to 2022 near $^{10}$Be sampling transect in Del Mar, California.

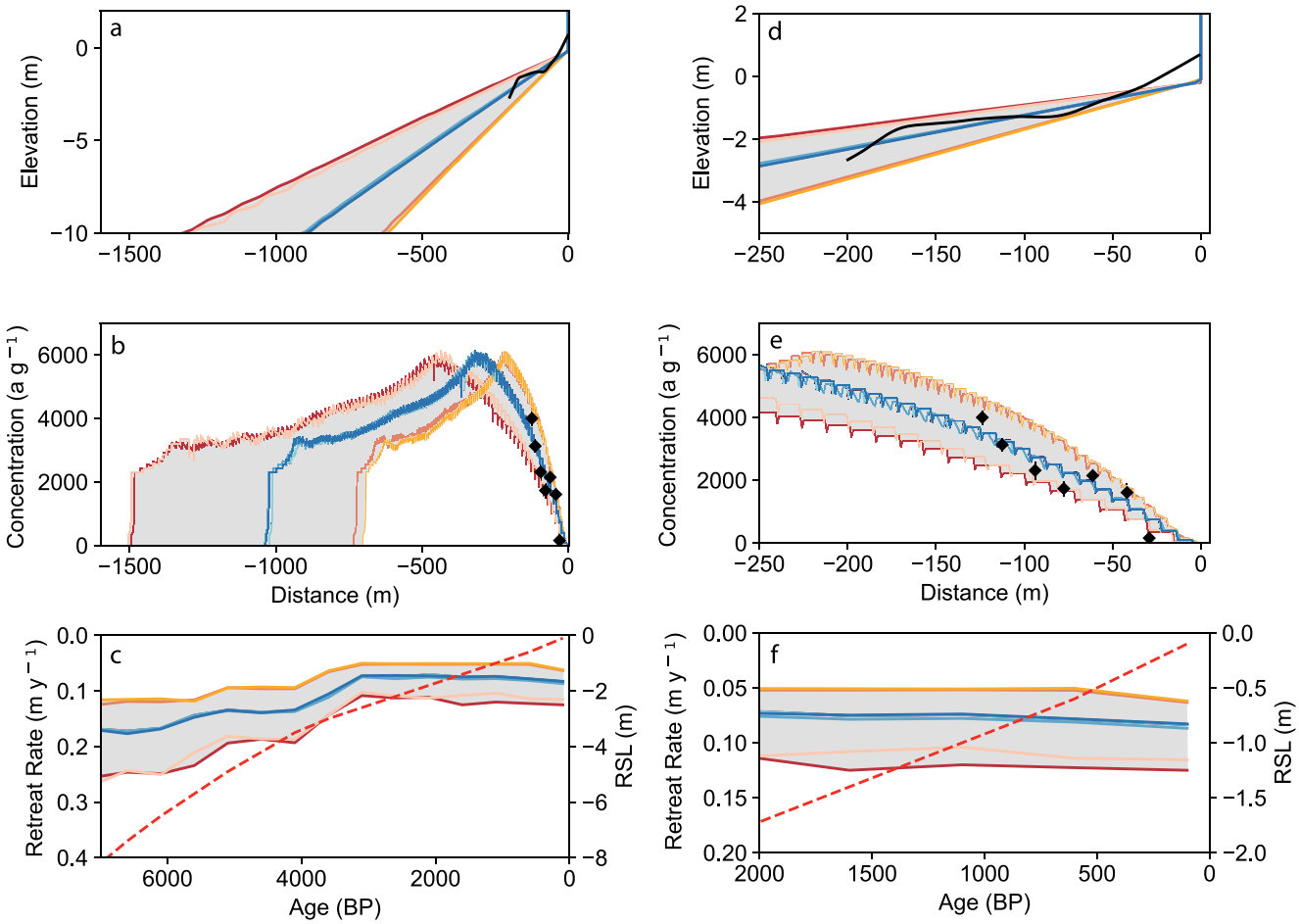


**Figure 5.** Final results from the multiobjective Markov Chain Monte Carlo modeling. The light blue line shows the best-fit results (i.e., calculated with the best-fit value for each parameter); two results from our uncertainty calculations virtually overlap with this result (dark blue lines), while four other results from our uncertainty calculations (warm-colored lines) show the upper and lower limits of the uncertainty range. Black diamonds represent measured cosmogenic concentrations from the shore platform, and the solid black lines represent the measured (combined) topographic and bathymetric profiles for the shore platform. Red dotted lines represent relative sea level over time (Reynolds & Simms, 2015). The first column shows the full width of the modeled topographic profile (a), $^{10}$Be cosmogenic profile (b), and the entire history of modeled cliff retreat rates from 7,000 years before present to present (c). The second column shows only the first 250 m of the modeled platform offshore from the cliff (d, e) and the last 2,000 years of modeled cliff retreat rates (Figure 4f).

transect is best constrained by the lowest concentration samples, as it is impossible for any sample along the transect to have a negative inheritance-corrected concentration. This inheritance treatment approach is also employed by M. D. Hurst et al. (2016) for their study sites.

### 3.2. Beach Sand Thickness

Average monthly beach elevation fluctuates up to about 1 m seasonally, with more eroded beaches in winter (Figure 4). Beach sand thickness shallows further away from the cliff, and the shore platform is often exposed during winter months. Typical sand thickness above the shore platform varies from 0 to ~1.5 m.

### 3.3. Multiobjective Optimization

#### 3.3.1. Best Fit Model Results

The best-fit parameters, their respective median, and 16%–84% confidence interval values (Table 5) are used to produce the modeled $^{10}$Be concentration and topographic profiles; model results show that a good fit is achieved against the measured $^{10}$Be concentration and topographic profiles (Figure 5). An acceptance rate of 27% was achieved for our MCMC analysis, close to that expected for a fully explored parameter space (~23%, Gelman et al., 1997). Acceptable material resistance (*Fr*) values, weathering rates (*K*), and wave height decay rates (*y*)

**Table 5**
*Best-Fit Parameter Results, Multiobjective Markov Chain Monte Carlo Calculations for Del Mar, CA*

| Wave height decay rate ($Y$) | | | | Material resistance ($Fr$) | | | | Weathering rate ($K$) | | | |
|---|---|---|---|---|---|---|---|---|---|---|---|
| $a$ (best fit) | $a$ (median) | $\pm$ (1$\sigma$) | $Y$ ($m^{-1}$) | $b$ (best fit) | $b$ (median) | $\pm$ (1$\sigma$) | $Fr$ (kg $m^{-2}$ $yr^{-1}$) | $c$ (best fit) | $c$ (median) | $\pm$ (1$\sigma$) | $K$ (kg $m^{-2}$ $yr^{-1}$) |
| −1.52 | −1.37 | 0.16 | **0.028–0.062** | 2.21 | 2.16 | 0.54 | **31.6–508.9** | −6.8 | −5.75 | 2.73 | **0.063–3.9** |
| | | −0.18 | | | | −0.54 | | | | −1.62 | |

*Note*. Bold indicates best-fit parameter ranges in "real world" values.

indicate that there is a large range in accepted material resistance and wave height decay rate values due to a correlation between material resistance and wave height decay (Table 5; Figure 6; Section 4.3), while any weathering rate below 2–200 kg $m^{-2}$ $yr^{-1}$ (for a given $Fr$ of 10–1,000 kg $m^{-2}$ $yr^{-1}$) achieves model acceptance. A best-fit model simulation is generated, with a cluster of two uncertainty simulations virtually overlapping with the best-fit model simulation, while the four other uncertainty simulations define the broader uncertainty envelope (Figure 5). This uncertainty envelope, and ultimately the range in reported modeled millennial cliff retreat rates, manifests primarily from the range in acceptable values for each parameter (Table 5). Topographic and cosmogenic profiles both show the maximum range and uncertainty furthest offshore the cliff, where there are no measured data to further constrain the profiles (Figures 5a and 5d). Closer to the cliff, where our field data and concentrations were measured, modeled cosmogenic profiles occupy a narrower range (±10%–20%) than distal from the cliff (±25%–30%) when comparing the modeled uncertainty profiles against the modeled best-fit profiles. Modeled topography decreases in elevation linearly from the cliff base and falls within the measured elevation uncertainty envelope for majority of the best-fit simulations. Modeled cosmogenic concentrations increase with distance from the cliff until a peak in concentration (M. D. Hurst et al., 2016, 2017; Regard et al., 2012) is reached 250–600 m offshore from the cliff; all modeled profiles then show decreases in cosmogenic concentrations for the remainder of the modeled distances.

The modeled topographic profiles also allow us to estimate the maximum width of the platform eroded over the course of the model run, suggesting 750–1,500 m in total has been eroded in 7,000 years (Figure 5a). Modeled cliff retreat rates from the simulations suggest that over the last ∼1,000–2,500 years BP, ∼125 m of shore platform has been eroded at this site (Figures 5d–5f). This is the distance over which we have measured cosmogenic data, and the time range over which we have the highest confidence in modeled retreat rates.

#### 3.3.2. Late Holocene Retreat Rates

Retreat rates over the length of the model simulation are calculated from the modeled cliff position every 100 years. Due to numerous simplifications (e.g., 100 years step size) of the modeling, we are unable to determine retreat rates at a finer resolution (e.g., 10-year intervals) without the manifestation of inaccurate irregularities in the results (i.e., large fluctuations in calculated retreat rate every decade). We note that due to the inherent assumption of no beach cover in the coupled model, these cliff retreat rates may be considered as maximum rates, as the effect of beach cover on the $^{10}$Be concentrations in Del Mar, unaccounted for in the implementation of RoBoCoP in the coupled numerical model, could be as high as ∼15% (see Section 4.2 for details). The first ∼1,000 years of the simulations correspond to the model burn-in period and are excluded from the analysis. An initial best-fit retreat rate of 11.5–26.4 cm $yr^{-1}$ is modeled at 7,000 years BP; this rate then decreases quasi linearly until ∼3,000 years BP, after which a nearly constant retreat rate of 5.0–12.0 cm $yr^{-1}$ is established until ∼1,000 years BP (Figure 5c). Retreat rates then begin to slowly increase to 6.2–12.5 cm $yr^{-1}$ until 100 years BP (Figure 5f). We are only able to confidently report retreat rates for the time period over which we have calibration data (∼2,000 years); however, our modeling suggests that the trajectory of the modeled cosmogenic concentrations cannot appreciably deviate from the observed trend until the characteristic hump, or peak in cosmogenic concentration, is reached without the model failing due to a substantial misfit with our measured data.

## 4. Discussion

### 4.1. Cosmogenic $^{10}$Be Concentrations

Cosmogenic concentrations increase with distance from the cliff base (except for CA-19-DLM-06), as expected from theory and prior experiments (e.g., M. D. Hurst et al., 2016, 2017; Regard et al., 2012). Our inheritance-corrected concentrations are relatively low (<4,000 at $g^{-1}$ $yr^{-1}$), suggesting that ∼125 m of the shore

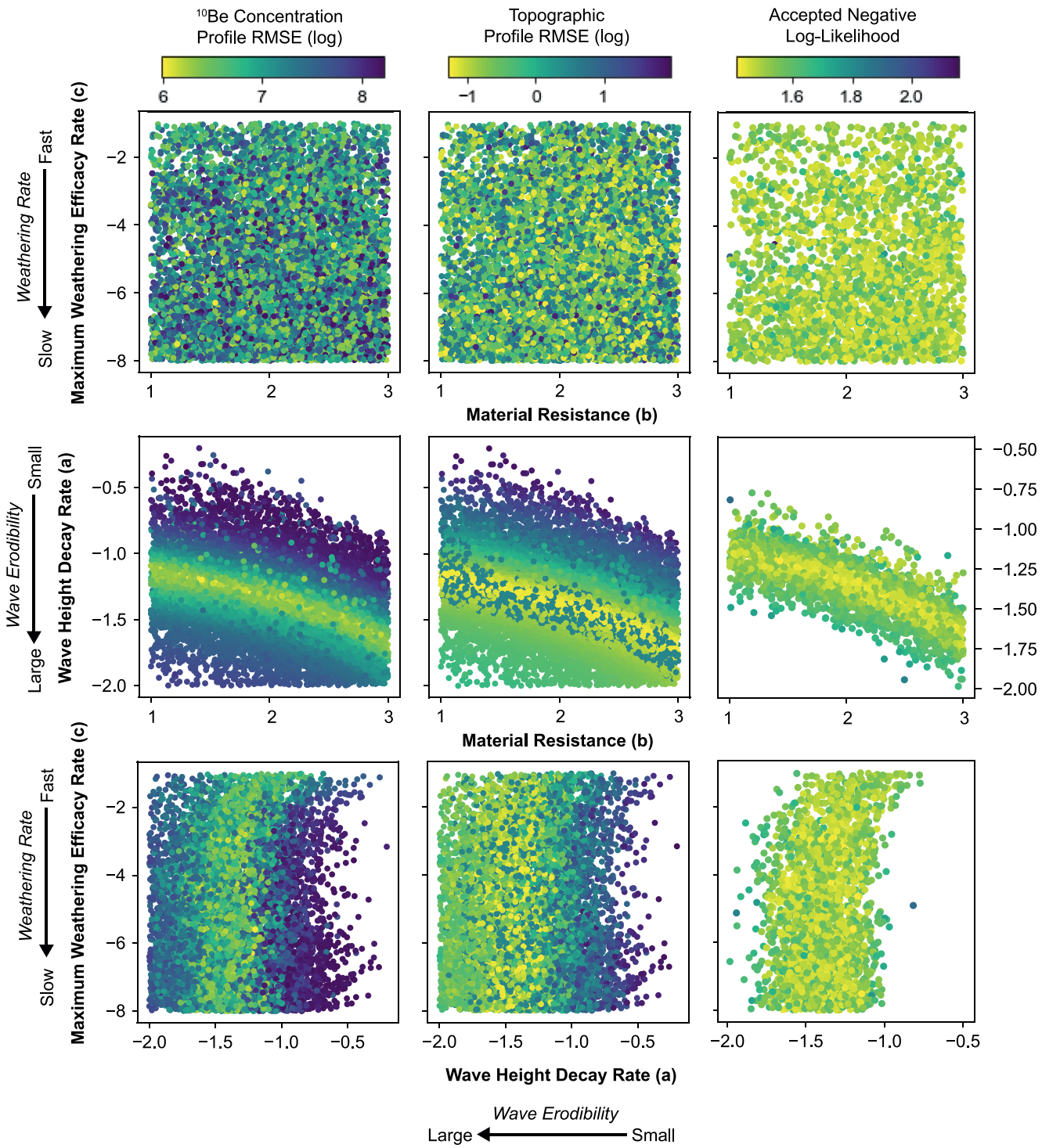


**Figure 6.** Markov Chain Monte Carlo (MCMC) model results comparing wave height decay rate (a), material resistance (b, larger values represent harder substrate), and weathering rate (c) parameters. The $^{10}$Be concentration profile (first column) and topographic profile root mean square error (RMSE) (second column) plots show results from all 10,000 iterations visited in the analysis, while the combined likelihood results (third column) show only those accepted ($n = 2{,}741$) from the model runs in the MCMC analysis. Dark blue circles correspond to model runs that result in the highest RMSE scores and negative log-likelihood scores, and thus poorly reproduce our measured data set, while bright yellow circles correspond to the model runs that result in the lowest RMSE and negative log-likelihood scores.

platform here was likely produced during the Holocene (Regard et al., 2012). Extrapolating from the slower end of modern day cliff retreat rates (~5 cm $yr^{-1}$) into the past, ~125 m of the shore platform would have developed in under three millennia, further suggesting mid-to-late Holocene development. The decrease in concentration observed between CA-19-DLM-05 and CA-19-DLM-06, deviating from the trend of increasing concentrations with distance from the cliff base, can most simply be explained either by nonuniform cliff retreat, as the samples are not exactly perpendicular to the cliff face, or by temporarily rapid cliff retreat at this junction, though the model is unable to resolve nuanced details of retreat in such a rapid time frame to test this hypothesis. Another possible explanation is a comparatively higher paleo-cliff height at this location, which would cause more attenuation of the cosmogenic signal, but such a cliff height increase would need to be sufficiently local in extent in order to not affect the concentrations of the proximal samples.

### 4.2. Beach Cover Effects

The coupled model employed in this study does not account for beach cover attenuation effects; M. D. Hurst et al. (2017) explored the effect of beach cover using their cosmogenic radionuclide production model (RoBoCoP) and found that extreme beach cover (1 m thick for >50 m width) is required to significantly reduce shore platform $^{10}$Be concentrations (i.e., by >15%). Given that observed beach thickness varies from about 0 to 1.5 m, with the thickest sand closest to the cliff, we consider the maximum effect of beach thickness on the shore platform concentrations to be ~15%. The coupled model inherently assumes no beach cover as a fixed property (Shadrick et al., 2021); we note again that our reported modeled cliff rates may be considered as maximum rates.

### 4.3. Model Results

In this section, we evaluate the efficacy of the model to resolve a reasonable match between measured and best-fit modeled data to better inform the validity of the modeled cliff retreat rates we report and also evaluate the suitability of this model for future limited shore platform data sets. Goodness of fit for the measured versus modeled $^{10}$Be concentrations and shore platform topographic profiles among the model runs is achieved for this site. Inheritance-corrected cosmogenic concentrations fall entirely within the modeled cosmogenic profile uncertainty envelope (Figures 5b and 5e). Our modeling suggests that the expected peak in cosmogenic concentrations for this platform will not be reached until ~215 m at minimum (Figure 5b). Measured topographic and bathymetric profiles mostly fall within the modeled topographic shore platform profile, with deviations up to ~1 m occurring closer to the cliff face (Figures 5a and 5d). These deviations are possibly related to our selection of areas locally high in elevation (i.e., sandstone nodules) and/or the model's incapability of simulating cliff-platform junction profiles. Importantly, the slope of the modeled platform gradients corresponds well with that measured (Figure 5d), providing confidence in the model results. These model results suggest that this methodology can successfully be used with a relatively limited cosmogenic data set (i.e., less than 10 samples) from a relatively narrow shore platform extent (<130 m) to simultaneously estimate cliff retreat over millennial timescales and evaluate the relative contributions of the primary drivers of coastal rocky cliff evolution, potentially increasing its utility in locations of similarly limited spatial extent. The applicability of this technique to other coastlines with narrow shore platforms may be limited in areas where the cliff erosion rates are so rapid that the concentrations of $^{10}$Be are indistinguishable given the uncertainty of the AMS measurements. Future improvements in AMS capabilities and the chemical isolation of $^{10}$Be would expand future applications. In addition, other cosmogenic nuclide systems such as in situ-produced $^{14}$C and/or $^{36}$Cl, which have higher cosmogenic nuclide production rates, may alleviate this challenge.

### 4.4. Parameter Correlation

Matsumoto et al. (2018) found that it is possible to produce similar topographic profiles across a range of intertidal weathering rates, material resistances, and wave height decay rates; we find similar model behaviors. Figure 6 shows correlation among the parameters (via varying the range in exponents applied to wave height decay rates ($y$), material resistance ($Fr$), and intertidal weathering rates ($K$)—$a$, $b$, and $c$, respectively—in the MCMC) we explore in the model as a function of the RMSE scores generated for the cosmogenic and topographic profiles from all simulations, as well as the negative log-likelihood of only the accepted coupled model simulations.

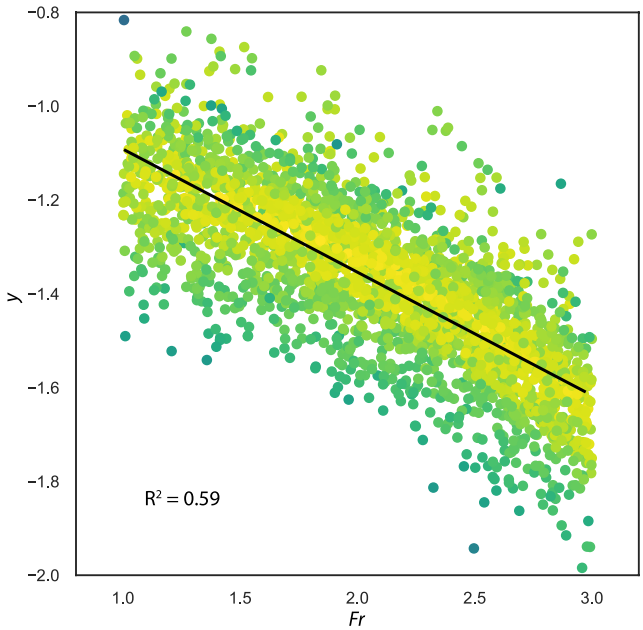


**Figure 7.** Plot of only accepted samples from the Markov Chain Monte Carlo analysis for material resistance (*Fr*, (b)) and wave height decay rate (*y*, (a)) parameters along with a linear regression calculation ($R^2 = -0.59$).

A comparison of modeled intertidal weathering rates (*c*) with material resistance (*b*) values indicates that once *c* falls below −1, model acceptance and low RMSE scores are achieved for both cosmogenic and topographic profiles. No distinctive trend in acceptance or RMSE scores is observed for any *c* below −1 for any value of *b*; this is expected as intertidal weathering rates vary as function of material resistance in the model. Comparing wave height decay (*a*) and intertidal weathering rates (*c*), the slowest wave height decay rates produce the most accurate topographic profiles, regardless of weathering rate. In other words, waves are eroding the shore platform across the widest possible distance for the slowest wave height dissipation rates as constrained by the chosen parameter ranges; however, the cosmogenic concentration profile RMSE scores reveal a nuanced interplay between these two factors in producing accepted model results. As wave height decay rate decreases, which ultimately increases the cross shore extent of wave erosion, slower intertidal weathering rates are needed to accurately match the measured data, indicating that less platform lowering occurs as wave-driven erosion increases. No distinct value for wave height decay rate nor intertidal weathering rate produces a model output that best matches our measured data; however, it is evident that wave height decay rates have a narrower acceptable range in comparison to intertidal weathering rates (which span five orders of magnitude) and thus a tighter control in reproducing the cosmogenic and topographic profiles (Table 5). Particularly at lower intertidal weathering rates, wave erosion and weathering trade off in a complex fashion to produce model outputs that simultaneously match the measured cosmogenic and topographic profiles. Our modeling suggests that while intertidal weathering is a necessary component in reproducing measured cosmogenic concentrations and topography, wave height decay rates exert a tighter control on model acceptance. Wave-driven erosion thus appears to provide a mechanism for relative sea level rise to exert an influence on cliff retreat rates in our modeled results, but further investigations are necessary to better understand the processes that affect shore platform development in Del Mar to corroborate these modeled inferences.

A negative linear relationship exists between modeled wave height decay rates and material resistance values (Figure 7), suggesting that a large range in material resistance values can achieve low RMSE scores for the cosmogenic profiles as well as model acceptance. As material resistance increases, more wave energy is needed (i.e., wave height decay rate needs to decrease) to erode the cliff fast enough to accurately reproduce the cosmogenic profile. This relationship exerts a control on the likelihood of acceptance in our modeling when optimizing for each profile simultaneously. A negative relationship between material resistance and wave height decay rate is similarly observed for the topographic profiles (Figure 6), but there is a much wider range for these variables that trends toward lower *y* and *Fr* values to achieve the lowest RMSE scores. This is likely a result of the shallow gradient of the platform; once *y* falls below −0.5, a shallow platform can be generated over a large range for *Fr* (i.e., the wave energy is high enough to erode the platform across a large range of material resistance values). While these tradeoffs and ranges of accepted parameters introduce a level of equifinality to our results, the combinations of wave height decay rate and material resistance values broadly follow a negative linear regression fitted to the accepted samples (Figure 7). This regression is similarly observed for the accepted samples in Shadrick et al. (2021); further, they found that across the negative *y*/*Fr* regressions of accepted samples for either of their sites, very similar retreat rate trajectories were produced. In conjunction with our results, this observation suggests that the modeled retreat rates here are plausable, despite the apparent equifinality.

### 4.5. Modern Versus Millennial Retreat Rates

Our modeling suggests that cliff retreat rates over the last two millennia in Del Mar range on average from 5.0–12.5 cm $yr^{-1}$ and fall within the same range as the measured recent retreat rates in the immediate vicinity (2–19 cm $yr^{-1}$, Figure 2, Benumof & Griggs, 1999; Hapke & Reid, 2007; Moore et al., 1999; Swirad & Young, 2022; Young, 2018; Young & Ashford, 2006; Young, Flick, et al., 2009; Young et al., 2021). Recent retreat rates in Del Mar that take into consideration multiple decades of data, from the 1930s to the 1990s, tend

to produce higher average retreat rates than those that measure retreat over shorter time intervals, though the ranges in reported rates for the latter encompass the former, highlighting the time variable nature of coastal cliff retreat in this area. The episodic nature of cliff retreat that produces variability among recent multidecadal versus subdecadal cliff retreat rates makes a direct comparison with modeled millennial retreat rates difficult, but the correspondence is remarkable and suggestive of well-constrained baseline cliff retreat behavior in Del Mar. Additionally, it appears that modeled cliff retreat rates have remained relatively constant from the late Holocene to ~1900, which is potentially a result of the relatively constant rate of RSL rise (Figure 5f). While prone to much greater uncertainty due to a lack of calibration data, modeled cliff retreat rates also appear to be higher when the rate of RSL rise was higher in the early to mid Holocene (Figure 5c). Nonetheless, this consistency among long- and short-term rates in Del Mar, California differs from other studies employing similar methodologies and found that a recent acceleration in cliff retreat rate has occurred (e.g., M. D. Hurst et al., 2016), while others find that the rate of RSL rise does not affect Holocene cliff retreat rates (e.g., Swirad et al., 2020). That the rate of RSL rise appears to influence modeled cliff retreat results here and not in other locations (e.g., North Yorkshire, UK; Swirad et al., 2020) might be a result of different relative influence of wave attack in driving erosion or may perhaps be related to local environmental variations (e.g., wave height, etc.); however, we are limited in our ability to probe further because our modeling does not consider the influence of potentially important local factors such as beach sediment thickness and rainfall. With the present model resolution limitations, we cannot ascertain the effect of recent RSL rise on modeled cliff retreat rates over the last ~100 years—the period over which RSL rise has approximately doubled in Southern California. Regardless, we speculate that perhaps there could be a lag time between RSL rise change and cliff retreat morphodynamics that is not reflected in our comparison nor in decadal retreat rate studies (Figure 2). Further investigations into modeled cliff retreat with finer resolution (i.e., finer grid cell size and model time step) and additional local factors, while complicated, could serve as an appropriate intermediator between long-term and short-term to properly assess the effects of RSL rise over shorter timescales.

## 5. Conclusion

In this study, we utilized cosmogenic in situ-produced $^{10}$Be concentrations and topographic measurements from a near-horizontal sandy claystone shore platform in Del Mar, San Diego County, California along with a multi-objective model optimization of a numerical model that couples cosmogenic production and coastal platform development to estimate late Holocene (~2,000 years) cliff retreat rates that range from 5.0 to 12.5 cm yr$^{-1}$. We demonstrate the ability to successfully utilize this new methodological approach with a relatively limited cosmogenic data set (i.e., nine samples over ~125 m of shore platform) to estimate retreat rates over millennial timescales, potentially opening up its feasibility in other rocky coast environments with limited topographic preservation and/or exposure. Modern observations (i.e., 0–100 years BP) of cliff top and cliff face retreat along this stretch of the California coast show average recent retreat rates of 2–19 cm yr$^{-1}$, suggesting that retreat rates have remained relatively constant over the last two millennia, but variability in average modern retreat rates over different time intervals (i.e., multidecadal vs. subdecadal) obscures this potential relationship. Modeled cliff retreat rates are relatively stable from ~3,000 to 100 years BP, a period characterized by a stable rate of relative sea level rise in Southern California. Our modeling treatment also allows us to qualitatively evaluate the relative influence of wave height decay rate, intertidal weathering, and material resistance in driving coastal evolution. Model acceptance is achieved over a range of values but requires both intertidal weathering and wave-driven erosion, the latter of which over a narrower parameter space (i.e., same order of magnitude), to reproduce the measured cosmogenic concentrations and topographic profile. All material resistance values have combinations that lead to model acceptance equally. These modeled observations imply that waves, and to a lesser degree intertidal weathering, exert a control on cliff retreat in Del Mar, and along with the modeled cliff retreat rates over the last two millennia, suggest that the rate of relative sea level might influence coastal cliff and shore platform erosion here, although further investigations are necessary because the present modeling ignores potentially important local factors (e.g., beach sediment, rainfall). Additional modeling at finer temporal and spatial resolution may help assess the effects of the recent (<100 years) approximate doubling in RSL rise in Southern California on cliff retreat.

## Data Availability Statement

All data necessary to reproduce the findings of this study are included in the main text. Plotting scripts, code, and documentation for the model can be found at https://doi.org/10.5281/zenodo.5645478 (M. Hurst et al., 2021).

**Acknowledgments**
Prepared in part by LLNL under Contract DE-AC52-07NA27344 and LLNL-JRNL-834640. APY was supported by the California Department of Parks and Recreation, Natural Resources Division Oceanography Program (C1670004 and C19E0049). HM was supported by U.S. Army Corps of Engineers (W912HZ1920020). The authors would also like to thank Dylan Rood and Martin Hurst for helpful comments and discussion, as well as Matt Brain, Mikaël Attal, and two anonymous reviewers for improving the quality of this work.

## References

Adams, B. M., Eldred, M. S., Geraci, G., Hooper, R. W., Jakeman, J. D., Maupin, K. A., et al. (2019). Dakota, A multilevel parallel object-oriented framework for design optimization, parameter estimation, uncertainty quantification, and sensitivity analysis: Version 6.10. User's Manual, 388.

Benumof, B. T., & Griggs, G. B. (1999). The dependence of seacliff erosion rates on cliff material properties and physical processes: San Diego County, California. *Shore and Beach*, *67*(4), 29–41.

Braucher, R., Brown, E. T., Bourlès, D. L., & Colin, F. (2003). In situ produced $^{10}$Be measurements at great depths: Implications for production rates by fast muons. *Earth and Planetary Science Letters*, *211*(3–4), 251–258. https://doi.org/10.1016/S0012-821X(03)00205-X

Brooks, S. M., & Spencer, T. (2010). Temporal and spatial variations in recession rates and sediment release from soft rock cliffs, Suffolk coast, UK. *Geomorphology*, *124*(1–2), 26–41. https://doi.org/10.1016/j.geomorph.2010.08.005

Buchanan, D. H., Naylor, L. A., Hurst, M. D., & Stephenson, W. J. (2020). Erosion of rocky shore platforms by block detachment from layered stratigraphy. *Earth Surface Processes and Landforms*, *45.4*(4), 1028–1037. https://doi.org/10.1002/esp.4797

California Natural Resources Agency. (2009). 2009 California Climate Adaptation Strategy, A Report to the Governor of the State of California in Response to Executive Order S-13-2008, (p. 200). Retrieved from https://resources.ca.gov/CNRALegacyFiles/docs/climate/Statewide_Adaptation_Strategy.pdf

Carr, A. P., & Graff, J. (1982). The tidal immersion factor and shore platform development: Discussion. *Transactions of the Institute of British Geographers*, *7*(2), 240–245. https://doi.org/10.2307/622227

Chmeleff, J., von Blanckenburg, F., Kossert, K., & Jakob, D. (2010). Determination of the $^{10}$Be half-life by multicollector ICP-MS and liquid scintillation counting. *Nuclear Instruments and Methods in Physics Research Section B: Beam Interactions with Materials and Atoms*, *268*(2), 192–199. https://doi.org/10.1016/j.nimb.2009.09.012

Dickson, M. E., Walkden, M. J., & Hall, J. W. (2007). Systemic impacts of climate change on an eroding coastal region over the twenty-first century. *Climatic Change*, *84*(2), 141–166. https://doi.org/10.1007/s10584-006-9200-9

Dornbusch, U., Robinson, D. A., Moses, C. A., & Williams, R. B. (2008). Temporal and spatial variations of chalk cliff retreat in East Sussex, 1873 to 2001. *Marine Geology*, *249*(3–4), 271–282. https://doi.org/10.1016/j.margeo.2007.12.005

Emery, K. O., & Kuhn, G. G. (1982). Sea cliffs: Their processes, profiles, and classification. *Geological Society of America Bulletin*, *93*(7), 644–654. https://doi.org/10.1130/0016-7606(1982)93<644:SCTPPA>2.0.CO;2

Estacio-Hiroms, K. C., Prudencio, E. E., Malaya, N. P., Vohra, M., & McDougall, D. (2016). The QUESO Library, User's Manual. arXiv preprint arXiv:1611.07521.

Flick, R. E. (1993). The myth and reality of southern California beaches. *Shore and Beach*, *61*(3), 3–13.

Gelman, A., Gilks, W. R., & Roberts, G. O. (1997). Weak convergence and optimal scaling of random walk Metropolis algorithms. *Annals of Applied Probability*, *7*(1), 110–120. https://doi.org/10.1214/aoap/1034625254

Gosse, J. C., & Phillips, F. M. (2001). Terrestrial in situ cosmogenic nuclides: Theory and application. *Quaternary Science Reviews*, *20*(14), 1475–1560. https://doi.org/10.1016/S0277-3791(00)00171-2

Griggs, G. B. (1998). California's coastline: El Nino: Erosion and protection. In L. Ewing & D. Sherman (Eds.), *California's coastal natural hazards* (pp. 36–55). University of Southern California.

Hapke, C. J., & Reid, D. (2007). *National assessment of shoreline change part 4: Historical coastal cliff retreat along the California coast*. (Open-File Report 2007-1133). U. S. Geological Survey.

Hurst, M., Matsumoto, H., Shadrick, J. R., Rood, D. H., & Dickson, M. E. (2021). mdhurst1/Rocky-Profile-Model: RPM-CRN with Dakota Implementation v1.0 (RPMV1.0) [code]. Zenodo. https://doi.org/10.5281/zenodo.5645478

Hurst, M. D., Rood, D. H., & Ellis, M. A. (2017). Controls on the distribution of cosmogenic $^{10}$Be across shore platforms. *Earth Surface Dynamics*, *5*(1), 67–84. https://doi.org/10.5194/esurf-5-67-2017

Hurst, M. D., Rood, D. H., Ellis, M. A., Anderson, R. S., & Dornbusch, U. (2016). Recent acceleration in coastal cliff retreat rates on the south coast of Great Britain. *Proceedings of the National Academy of Sciences of the United States of America*, *113*(47), 13336–13341. https://doi.org/10.1073/pnas.1613044113

IPCC. (2021). Climate change 2021: The physical science basis. In V. Masson-Delmotte, P. Zhai, A. Pirani, S. L. Connors, C. Péan, et al. (Eds.), *Sixth assessment report of the intergovernmental panel on climate change*. Cambridge University Press.

Kanyaya, J. I., & Trenhaile, A. S. (2005). Tidal wetting and drying on shore platforms: An experimental assessment. *Geomorphology*, *70*(1–2), 129–146. https://doi.org/10.1016/j.geomorph.2005.04.005

Kennedy, D. M., Paulik, R., & Dickson, M. E. (2011). Subaerial weathering versus wave processes in shore platform development: Reappraising the Old Hat Island evidence. *Earth Surface Processes and Landforms*, *36*(5), 686–694. https://doi.org/10.1002/esp.2092

Kennedy, D. M., Stephenson, W. J., & Naylor, L. A. (2014). Chapter 1 introduction to the rock coasts of the world, geological society. *London, Memoirs*, *40*, 1–5. https://doi.org/10.1144/M40.1

Kennedy, M. P. (1975). Geology of the western San Diego metropolitan area, California: Del Mar, La Jolla, and point loma quadrangles. *California Division of Mines and Geology Bulletin. A*, *200*, 709–722.

Kern, J. P., & Rockwell, T. K. (1992). Chronology and deformation of quaternary marine shorelines, San Diego County, California. In E. Heath & L. Lewis (Eds.), *The regressive Pleistocene shoreline in southern California: Santa Ana, California* (pp. 1–7). South Coast Geological Society. Annual Field Trip Guidebook 20.

Kline, S. W., Adams, P. N., & Limber, P. W. (2014). The unsteady nature of sea cliff retreat due to mechanical abrasion, failure and comminution feedbacks. *Geomorphology*, *219*, 53–67. https://doi.org/10.1016/j.geomorph.2014.03.037

Kohl, C. P., & Nishiizumi, K. (1992). Chemical isolation of quartz for measurement of in-situ-produced cosmogenic nuclides. *Geochimica et Cosmochimica Acta*, *56*(9), 3583–3587. https://doi.org/10.1016/0016-7037(92)90401-4

Korschinek, G., Bergmaier, A., Faestermann, T., Gerstmann, U. C., Knie, K., Rugel, G., et al. (2010). A new value for the half-life of $^{10}$Be by heavy-ion elastic recoil detection and liquid scintillation counting. *Nuclear Instruments and Methods in Physics Research Section B: Beam Interactions with Materials and Atoms*, *268*(2), 187–191. https://doi.org/10.1016/j.nimb.2009.09.020

Kuhn, G. G., & Osborne, R. H. (1987). Sea cliff erosion in San Diego County, California. In N. C. Kraus (Ed.), *Coastal sediments* (pp. 1839–1854). American Society of Civil Engineers.

Kuhn, G. G., & Shepard, F. P. (1984). *Sea cliffs, beaches, and coastal valleys of San Diego county: Some amazing histories and some horrifying implications* (pp. 1–193). University of California Press.
Lal, D. (1991). Cosmic ray labeling of erosion surfaces: In situ nuclide production rates and erosion models. *Earth and Planetary Science Letters*, *104*(2–4), 424–439. https://doi.org/10.1016/0012-821X(91)90220-C
Limber, P. W., Barnard, P. L., Vitousek, S., & Erikson, L. H. (2018). A model ensemble for projecting multidecadal coastal cliff retreat during the 21st century. *Journal of Geophysical Research: Earth Surface*, *123*(7), 1566–1589. https://doi.org/10.1029/2017JF004401
Ludka, B. C., Guza, R. T., O'Reilly, W. C., Merrifield, M. A., Flick, R. E., Bak, A. S., et al. (2019). Sixteen years of bathymetry and waves at San Diego beaches. *Scientific Data*, *6*(1), 1–13. https://doi.org/10.1038/s41597-019-0167-6
Matsumoto, H., Dickson, M. E., & Kench, P. S. (2016). An exploratory numerical model of rocky shore profile evolution. *Geomorphology*, *268*, 98–109. https://doi.org/10.1016/j.geomorph.2016.05.017
Matsumoto, H., Dickson, M. E., & Kench, P. S. (2018). Modeling the relative dominance of wave erosion and weathering processes in shore platform development in micro-to mega-tidal settings. *Earth Surface Processes and Landforms*, *43*(12), 2642–2653. https://doi.org/10.1002/esp.4422
McElroy, B., Willenbring, J. K., & Mohrig, D. (2018). Addressing time-scale–dependent erosion rates from measurement methods with censorship. *Geological Society of America Bulletin*, *130*(3–4), 381–395. https://doi.org/10.1130/B31644.1
Moore, L. J., Benumof, B. T., & Griggs, G. B. (1999). Coastal erosion hazards in Santa Cruz and San Diego Counties, California. *Journal of Coastal Research*, 121–139.
Muhs, D. R., Simmons, K. R., Schumann, R. R., Groves, L. T., Mitrovica, J. X., & Laurel, D. (2012). Sea-level history during the last interglacial complex on San Nicolas Island, California: Implications for glacial isostatic adjustment processes, paleozoogeography and tectonics. *Quaternary Science Reviews*, *37*, 1–25. https://doi.org/10.1016/j.quascirev.2012.01.010
Naylor, L. A., Coombes, M. A., & Viles, H. A. (2012). Reconceptualising the role of organisms in the erosion of rock coasts: A new model. *Geomorphology*, *157*, 17–30. https://doi.org/10.1016/j.geomorph.2011.07.015
Naylor, L. A., Stephenson, W. J., & Trenhaile, A. S. (2010). Rock coast geomorphology: Recent advances and future research directions. *Geomorphology*, *114*(1–2), 3–11. https://doi.org/10.1016/j.geomorph.2009.02.004
Nishiizumi, K., Imamura, M., Caffee, M. W., Southon, J. R., Finkel, R. C., & McAninch, J. (2007). Absolute calibration of $^{10}$Be AMS standards. *Nuclear Instruments and Methods in Physics Research Section B: Beam Interactions with Materials and Atoms*, *258*(2), 403–413. https://doi.org/10.1016/j.nimb.2007.01.297
Ogawa, H., Dickson, M. E., & Kench, P. S. (2011). Wave transformation on a sub-horizontal shore platform, Tatapouri, North Island, New Zealand. *Continental Shelf Research*, *31*(14), 1409–1419. https://doi.org/10.1016/j.csr.2011.05.006
Prémaillon, M., Regard, V., Dewez, T. J. B., & Auda, Y. (2018). GlobR2C2 (global recession rates of coastal cliffs): A global relational database to investigate coastal rocky cliff erosion rate variations. *Earth Surface Dynamics*, *6*, 651–668. https://doi.org/10.5194/esurf-6-651-2018
Regard, V., Dewez, T., Bourlès, D. L., Anderson, R. S., Duperret, A., Costa, S., et al. (2012). Late Holocene seacliff retreat recorded by $^{10}$Be profiles across a coastal platform: Theory and example from the English Channel. *Quaternary Geochronology*, *11*, 87–97. https://doi.org/10.1016/j.quageo.2012.02.027
Reynolds, L. C., & Simms, A. R. (2015). Late Quaternary relative sea level in southern California and Monterey Bay. *Quaternary Science Reviews*, *126*, 57–66. https://doi.org/10.1016/j.quascirev.2015.08.003
Shadrick, J. R., Hurst, M. D., Piggott, M. D., Hebditch, B. G., Seal, A. J., Wilcken, K. M., & Rood, D. H. (2021). Multi-objective optimisation of a rock coast evolution model with cosmogenic $^{10}$Be analysis for the quantification of long-term cliff retreat rates. *Earth Surface Dynamics*, *9*(6), 1505–1529. https://doi.org/10.5194/esurf-9-1505-2021
Small, C., & Nicholls, R. J. (2003). A global analysis of human settlement in coastal zones. *Journal of Coastal Research*, 584–599.
Sunamura, T. (1992). *Geomorphology of rocky coasts* (Vol. 3). John Wiley & Son Ltd.
Sunamura, T. (1994). Rock control in coastal geomorphic processes. *Transactions - Japanese Geomorphological Union*, *15*, 253–272.
Sunamura, T. (2015). Rocky coast processes: With special reference to the recession of soft rock cliffs. *Proceedings of the Japan Academy, Series B*, *91*(9), 481–500. https://doi.org/10.2183/pjab.91.481
Swirad, Z. M., Rosser, N. J., & Brain, M. J. (2019). Identifying mechanisms of shore platform erosion using Structure-from-Motion (SfM) photogrammetry. *Earth Surface Processes and Landforms*, *44*(8), 1542–1558. https://doi.org/10.1002/esp.4591
Swirad, Z. M., Rosser, N. J., Brain, M. J., Rood, D. H., Hurst, M. D., Wilcken, K. M., & Barlow, J. (2020). Cosmogenic exposure dating reveals limited long-term variability in erosion of a rocky coastline. *Nature Communications*, *11*(1), 1–9. https://doi.org/10.1038/s41467-020-17611-9
Swirad, Z. M., & Young, A. P. (2022). Spatial and temporal trends in California coastal cliff retreat. *Geomorphology*, *412*, 108318. https://doi.org/10.1016/j.geomorph.2022.108318
Trenhaile, A. S. (2000). Modeling the development of wave-cut shore platforms. *Marine Geology*, *166*(1–4), 163–178. https://doi.org/10.1016/S0025-3227(00)00013-X
Trenhaile, A. S. (2008). Modeling the role of weathering in shore platform development. *Geomorphology*, *94*(1–2), 24–39. https://doi.org/10.1016/j.geomorph.2007.04.002
von Blanckenburg, F., Hewawasam, T., & Kubik, P. W. (2004). Cosmogenic nuclide evidence for low weathering and denudation in the wet, tropical highlands of Sri Lanka. *Journal of Geophysical Research*, *109*(F3), F03008. https://doi.org/10.1029/2003JF000049
Willis, C. M., & Griggs, G. B. (2003). Reductions in fluvial sediment discharge by coastal dams in California and implications for beach sustainability. *The Journal of Geology*, *111*(2), 167–182. https://doi.org/10.1086/345922
Young, A. P. (2015). Recent deep-seated coastal landsliding at San Onofre State Beach, California. *Geomorphology*, *228*, 200–212. https://doi.org/10.1016/j.geomorph.2014.08.005
Young, A. P. (2018). Decadal-scale coastal cliff retreat in southern and central California. *Geomorphology*, *300*, 164–175. https://doi.org/10.1016/j.geomorph.2017.10.010
Young, A. P., & Ashford, S. A. (2006). Application of airborne LIDAR for seacliff volumetric change and beach-sediment budget contributions. *Journal of Coastal Research*, *22*(2), 307–318. https://doi.org/10.2112/05-0548.1
Young, A. P., & Carilli, J. E. (2019). Global distribution of coastal cliffs. *Earth Surface Processes and Landforms*, *44*(6), 1309–1316. https://doi.org/10.1002/esp.4574
Young, A. P., Flick, R. E., Gutierrez, R., & Guza, R. T. (2009). Comparison of short-term seacliff retreat measurement methods in Del Mar, California. *Geomorphology*, *112*(3–4), 318–323. https://doi.org/10.1016/j.geomorph.2009.06.018
Young, A. P., Guza, R. T., Flick, R. E., O'Reilly, W. C., & Gutierrez, R. (2009). Rain, waves, and short-term evolution of composite seacliffs in southern California. *Marine Geology*, *267*(1–2), 1–7. https://doi.org/10.1016/j.margeo.2009.08.008
Young, A. P., Guza, R. T., Matsumoto, H., Merrifield, M. A., O'Reilly, W. C., & Swirad, Z. M. (2021). Three years of weekly observations of coastal cliff erosion by waves and rainfall. *Geomorphology*, *375*, 107545. https://doi.org/10.1016/j.geomorph.2020.107545

Young, A. P., Guza, R. T., O'Reilly, W. C., Burvingt, O., & Flick, R. E. (2016). Observations of coastal cliff base waves, sand levels, and cliff top shaking. *Earth Surface Processes and Landforms*, *41*(11), 1564–1573. https://doi.org/10.1002/esp.3928

Young, A. P., Raymond, J. H., Sorenson, J., Johnstone, E. A., Driscoll, N. W., Flick, R. E., & Guza, R. T. (2010). Coarse sediment yields from seacliff erosion in the Oceanside littoral cell. *Journal of Coastal Research*, *26*(3), 580–585. https://doi.org/10.2112/08-1179.1

Yuan, R., Kennedy, D. M., Stephenson, W. J., & Finlayson, B. L. (2020). The multidecadal spatial pattern of erosion on sandstone shore platforms in south-eastern Australia. *Geomorphology*, *371*, 107437. https://doi.org/10.1016/j.geomorph.2020.107437